Adaptive Equilibrium Regulation: Modeling Individual Dynamics on Multiple Timescales

McKee, Kevin L.*
mckeek@vcu.edu
(703) 593-1690

Rappaport, Lance M.*
lance.rappaport@vcuhealth.org
(804) 828-8137

Boker, Steven M.**
smb3u@virginia.edu
(434) 243-7275

Moskowitz, D. S.***
debbie.moskowitz@mcgill.ca
(514) 398-6108

Neale, Michael C.*
michael.neale@vcuhealth.org
(804) 828-3369

*Virginia Commonwealth University
Virginia Institute of Psychiatric and Behavioral Genetics
800 E. Leigh St.
Richmond, VA, USA 23298-0126

**University of Virginia
Department of Psychology
020 Gilmer Hall
Charlottesville, VA, USA 22903

***McGill University
Department of Psychology
2001 McGill College
Montreal, QC, Canada H3A 1G1

Abstract

Damped Linear Oscillators estimated by 2nd-order Latent Differential Equation (LDE) have assumed a constant equilibrium and one oscillatory component. Lower-frequency oscillations may come from seasonal background processes, which non-randomly contribute to deviation from equilibrium at each occasion and confound estimation of dynamics over shorter timescales. Boker (2015) proposed a model of individual change on multiple timescales, but implementation, simulation, and applications to data have not been demonstrated. This study implemented a generalization of the proposed model; examined robustness to varied timescale ratios, measurement error, and occasions-per-person in simulated data; and tested for dynamics at multiple timescales in experience sampling affect data. Results show small standard errors and low bias to dynamic estimates at timescale ratios greater than 3:1. Below 3:1, estimate error was sensitive to noise and total occasions; rates of non-convergence increased. For affect data, model comparisons showed statistically significant dynamics at both timescales for both participants.

Introduction

Background

Many physiological and psychological processes can be described as self-regulating feedback control systems in which a steady state is maintained through continual adjustments, or negative feedback. For example, in postural control, negative feedback is provided by vision and proprioception, such that one moderates the force exerted by differential muscle groups via a sense of absolute position in space. Negative feedback that moderates a person's behavior comes from a variety of sources including negative social consequences, impacts to the person's health, and unpleasant states of affect. The trajectories of self-regulating processes can be modeled by a variety of methods, including time and frequency domain models (e.g., Wei, 2006). Dynamical Systems Analysis (DSA) has been advocated to provide parameterizations of change that better represent feedback control as it is found in living systems (Barton, 1994; Boker, 2002). DSA has seen a growing variety of applications to time series data in the life sciences and medical research where they have been used, for example, to model cognitive response patterns (Smith, 2000), postural control (Oie et al., 2002), regulation of emotions in non-clinical populations (Chow et al., 2005; Oravecz et al., 2011) as well as in borderline personality disorder (Ebner-Priemer et al., 2015), patterns of nicotine and alcohol use (Boker and Graham, 1998), ovarian hormone cycles (Boker et al., 2014), and to link hormone cycles to negative affect and eating behavior (Hu et al., 2014).

Dynamical systems can be modeled by fitting a stochastic differential equation (SDE) to data. SDEs differ from ordinary differential equations and other deterministic systems in that their solutions, called diffusion processes, may include random components as well as superposed, random error variation (Tuma and Hannan, 1984). Some SDEs may not have unique or any solutions. Latent Differential Equations (LDE) (Boker et al., 2004) present one possible method for handling these cases by using structural equation modeling (SEM) with latent variables (e.g., Bollen, 1989) to estimate parameters from the covariance structure of the derivatives without requiring a solution to the SDE. For the current study, we focused on a special case of the LDE, the 2nd-order damped linear oscillator (DLO) (Chow et al., 2005). The DLO describes patterns of variation as a function of deviation from equilibrium, and so is a suitable choice for modeling the behavior of feedback control systems.

Most applications of the damped linear oscillator have assumed a static or linearly changing equilibrium, but for complex, living systems, the assumption becomes less tenable as data are collected over longer spans of time. Taking for instance, affect in individuals suffering Bipolar or Seasonal Affective Disorder (Rosenthal et al., 1984), in which the mean level of negative affect varies according to prolonged episodes or seasonal conditions. The short-term dynamics of affect within a season are of a different nature and timescale from those which determine the mean level of each season. For processes such as these where equilibrium exhibits complex patterns of non-stationarity, the basic specification of the DLO is insufficient. Unmodeled, long-term background processes will non-randomly contribute to the overall deviation from equilibrium at each occasion and confound the estimation of dynamics over shorter timescales. To accurately estimate the parameters of damped oscillation at one particular timescale, a higher-order system that accounts for seasonality at longer timescales must be specified. Boker (2015) proposed an extension of the LDE to include a dynamic equilibrium, titled Adaptive Equilibrium Regulation (AER), but SEM implementation, simulations, and applications have not yet been demonstrated.

We propose a generalization of the AER model to estimate dynamics at multiple, nested timescales to account for gradual change in equilibrium. We hypothesized: 1) That the model would be able to estimate multiple frequency and damping parameters within a univariate series, given the presence of sufficiently distinct timescales as oscillation frequencies; 2) Additional timescales would play a statistically significant role in intra-individual affect variability and influence the estimation of short-term affect dynamics. Simulations were used to evaluate the precision and accuracy of model estimates for various long-to-short timescale ratios, signal-to-noise[1] ratios, and number of measurement occasions per person. Second, the model was applied to experience sampling affect data for two individuals to determine the significance of the additional dynamics.

Modeling Approaches

To describe a damped linear oscillator, we can use a 2nd-order differential equation of the following form:

$$\ddot{x}(t) = \eta x(t) + \zeta \dot{x}(t) \tag{1}$$

This equation is suitable for describing a simple relationship whereby acceleration ($\ddot{x}$) is linearly related to velocity ($\dot{x}$) and position (x). Coefficient η is the primary determinant of the frequency of oscillation. Because η is the proportion relating deviation from equilibrium to acceleration, it must necessarily be negative for the equilibrium to behave as an attractor toward which x will always accelerate. For discrete time, η can be calculated as a function of intervals per cycle, λ, as

[1] In all occurrences, we use the term 'noise' to refer to superposed, i.i.d., random variation such as measurement error, as distinct from stochastic variation in the signal, otherwise known as dynamic error.

follows[2]:

$$\lambda = 2\pi\sqrt{-1/\eta + \zeta^2/4} \qquad\qquad \eta = -\left(\frac{2\pi}{\lambda}\right)^2 - \zeta^2/4 \tag{2}$$

The velocity coefficient ζ determines the magnitude and sign of feedback. If ζ is negative, then the system will exhibit damped behavior. That is, wave amplitudes will diminish as time passes from the initial conditions. If ζ is positive, the oscillations will amplify over time. For low enough negative values of ζ, the system will not exhibit oscillation at all, instead returning to equilibrium monotonically. We can calculate ζ as a function of η and Δ, the natural log of the ratio between any two consecutive peaks x_0 and x_1 in a series of oscillations:

$$\Delta = ln(x_1/x_0) = \frac{\pi\zeta}{\sqrt{-\eta}} \qquad\qquad \zeta = \frac{\Delta\sqrt{-\eta}}{\pi} \tag{3}$$

To model a series of data according to this form, derivatives must be estimated. In the next sections, we review Generalized Local Linear Approximation (GLLA) (Boker et al., 2010) as the basis for constructing the LDE.

Generalized Local Linear Approximation

GLLA estimates the derivatives of a discrete series by assuming each observed datum represents a point along some underlying, continuously differentiable function, $x(t)$. The derivatives of $x(t)$ are estimated from neighborhoods of observed data in Y. To do this, a time-embedded matrix of the data is constructed in which each row contains D equally-spaced[3] occasions over the index intervals τ. The neighborhood of D points is referred to as the time-embedding window. To clarify, let us define i as the global index for each of N measurement occasions in Y:

$$y_i \in \mathrm{Y}, \qquad i \in \{0...N-1\} \tag{4}$$

The time-embedded matrix $\mathrm{Y}^{(D)}$ is then defined as:

$$\mathrm{Y}^{(D)} = \begin{bmatrix} y_0 & y_\tau & y_{2\tau} & \cdots & y_{\tau(D-1)} \\ y_1 & y_{1+\tau} & y_{1+2\tau} & \cdots & y_{1+\tau(D-1)} \\ y_2 & y_{2+\tau} & y_{2+2\tau} & \cdots & y_{2+\tau(D-1)} \\ \vdots & \vdots & \vdots & \ddots & \vdots \\ y_{N-\tau(D-1)} & \cdots & y_{n-2\tau} & y_{n-\tau} & y_N \end{bmatrix} \tag{5}$$

D and τ can be chosen such that the dependence of y_i upon preceding lags is encapsulated within each row of the data. If an even value of D is chosen, no single measurement occasion provides a value for exactly the same time as the estimated x_t. The window, and hence the derivative estimates, will be centered between occasions. If occasions are equally spaced in time, then given an initial time value for the series t_0 and the time interval Δt:

$$y_t \in \mathrm{Y}, \qquad t = t_0 + i\Delta t \tag{6}$$

We can then define the local, symmetrical time lags and leads $l(j)$ as a function of the local index j of each occasion within the embedding window:

$$l(j) = \tau\Delta t(j - \mathbb{E}[\mathrm{J}]), \qquad j \in \mathrm{J} = \{1, 2, ..., D\} \tag{7}$$

Here, the difference of each index in the time-embedding window from their mean value is taken and scaled by the index and time intervals. This gives us a definition of the time-embedding window at time t with its associated lags and leads as $y_{t+l(j)}$. The first half of $l(j)$ will produce negative time offsets (lags) and the second half will produce positive time offsets (leads). The convenience of this definition becomes clearer when we have to relate the indices of each occasion to their places in real time. Furthermore, derivatives of the underlying trajectory X are estimated to occur at the center of the embedding window, time t, not at each occasion i. This way, the time-embedding window is generalized to allow for both even and odd values of D while retaining time symmetry.

To estimate the derivatives of X up to the 2nd order, each row of $Y^{(D)}$ can be projected onto a $D \times 3$ matrix L of basis vectors approximating an 2nd order polynomial over the window $y_{t+l(j)}$:

$$\mathrm{L} = \begin{array}{c} \\ y_{t+l(1)} \\ y_{t+l(2)} \\ \vdots \\ y_{t+l(D)} \end{array} \begin{array}{c} \begin{array}{ccc} x & \dot{x} & \ddot{x} \end{array} \\ \begin{bmatrix} 1 & l(1) & l(1)^2/2 \\ 1 & l(2) & l(2)^2/2 \\ \vdots & \vdots & \vdots \\ 1 & l(D) & l(D)^2/2 \end{bmatrix} \end{array} \tag{8}$$

[2]For the simulations in this study, values of ζ were sufficiently small, and timescale ratios were approximate and randomly varied, such that both terms $\pm\zeta^2/4$ were excluded from calculations.

[3]Compatible techniques for data with irregular intervals have been developed (See: Tiberio, 2008).

The first column represents a constant value, and each subsequent column contains the indefinite integral of the preceding. Following the algebra for ordinary least squares, we take W, the pseudoinverse of L, and post-multiply $Y^{(D)}$ to obtain the matrix of estimated derivatives X:

$$\mathrm{Y}^{(D)} = \mathrm{XL}^T \tag{9}$$
$$\mathrm{Y}^{(D)}\mathrm{L}(\mathrm{L}^T\mathrm{L})^{-1} = \mathrm{XL}^T\mathrm{L}(\mathrm{L}^T\mathrm{L})^{-1} \tag{10}$$
$$\mathrm{Y}^{(D)}\mathrm{L}(\mathrm{L}^T\mathrm{L})^{-1} = \mathrm{X} \tag{11}$$
$$\mathrm{W} = \mathrm{L}(\mathrm{L}^T\mathrm{L})^{-1} \tag{12}$$
$$\mathrm{Y}^{(D)}\mathrm{W} = \mathrm{X} \tag{13}$$

For simple feedback control systems, we would be interested in fitting a 2nd-order differential equation to the series Y. Following the steps for GLLA, we would then have the matrix X of derivatives up to order 2, and could then model a linear dependence of the 2nd derivative on the 0th and 1st.

Latent Differential Equations

Unlike GLLA, LDEs do not estimate derivatives directly. Instead, the covariance structure of the embedded data $Y^{(D)}$ is described by the linear interrelations between the latent variances of the derivatives. This model is shown as a path diagram in Figure 1, with the latent derivatives as circles and the time-embedded data as squares. The curved, two-headed arrows represent the estimated variances and covariances of each component, while single-headed arrows represent linear regression coefficients. Bolded, labeled arrows are the freely estimated parameters. Latent variables can be specified to estimate the variance of linear approximations by fixing their paths (the narrow, single-headed arrows) to each occasion in the time embedding window to the approximations used by GLLA. The matrix L of these fixed factor loading values is specified exactly according to equation (8).

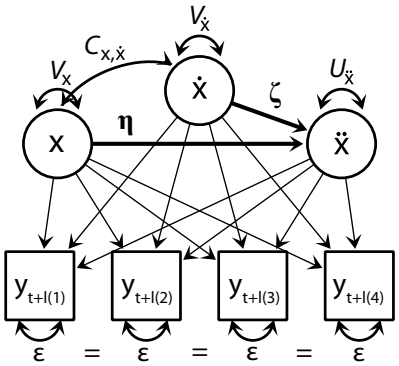

Figure 1: Damped Linear Oscillator as a 2nd-order Latent Differential Equation

The expected covariance of the time-embedded data computed from the model shown in Figure 1 can be specified with algebra generalizing factor analysis, such as RAM notation (McArdle and McDonald, 1984). We used a modification of RAM for faster matrix inversion:

$$\hat{\Sigma}(\theta) = \mathrm{L}(\mathrm{I} - \mathrm{A})^{-1}\mathrm{S}(\mathrm{I} - \mathrm{A})^{-1T}\mathrm{L}^T + \mathrm{E} \tag{14}$$

For D time-embedded columns of the manifest variable and q latent variables, $\hat{\Sigma}(\theta)$ is a $D \times D$ estimated autocovariance matrix of the observed variable as a function of θ, a vector of estimated parameters. S is a $q \times q$ covariance matrix of the latent variables, with variances along the diagonal.

$$\mathrm{S} = \begin{bmatrix} V_x & C_{x,\dot{x}} & 0 \\ C_{x,\dot{x}} & V_{\dot{x}} & 0 \\ 0 & 0 & U_{\ddot{x}} \end{bmatrix} \tag{15}$$

Here, V_x and $V_{\dot{x}}$ are the latent variances of the 0th and 1st derivatives. Because the 2nd derivative is modeled to be a linear combination of the first two, $U_{\ddot{x}}$ is any additional, unexplained variance attributable to stochastic variation in the signal.

The $q \times q$ matrix A contains regression coefficients between latent variables, with each located along the row of the dependent variable and the column of the independent variable. I is a $q \times q$ identity matrix, and E is the $D \times D$ diagonal

matrix of estimated residual variance or measurement error. The residual variance is assumed to remain stationary, so the same variance is estimated for all columns of the time-embedded variable.

$$\mathrm{A} = \begin{array}{c} \\ x \\ \dot{x} \\ \ddot{x} \end{array} \begin{array}{c} \begin{array}{ccc} x & \dot{x} & \ddot{x} \end{array} \\ \begin{bmatrix} 0 & 0 & 0 \\ 0 & 0 & 0 \\ \eta & \zeta & 0 \end{bmatrix} \end{array} \qquad \mathrm{E} = \begin{array}{c} \\ y_{t+l(1)} \\ \vdots \\ y_{t+l(D)} \end{array} \begin{array}{c} \begin{array}{ccc} y_{t+l(1)} & \cdots & y_{t+l(D)} \end{array} \\ \begin{bmatrix} \epsilon & 0 & 0 \\ 0 & \ddots & 0 \\ 0 & 0 & \epsilon \end{bmatrix} \end{array} \tag{16}$$

We will return to the specification of these models in more detail in the methods section. For more general information about specifying LDEs and choosing an embedding dimension, see (Boker, 2012).

Adaptive Equilibrium Regulation

An extension of the Latent Differential Equation model was proposed by Boker (2015) to model variability across multiple timescales. Named Adaptive Equilibrium Regulation (AER), this model allows equilibrium to exhibit its own regulatory patterns on a higher-order timescale. To do this, it uses a large enough embedding window to describe gradual change while fitting a second model at equally sized, smaller subset windows to describe short-term change. In other words, the long-term model describes the non-stationary equilibrium of the short-term model, and the short-term model describes time-dependence in residuals from the long-term model. This model represents a 4^{th}-order oscillating system parameterized for convenient interpretation as two nested 2nd-order systems.

A general version of AER is shown in Figure 2. Figure 2a shows the fixed regression paths specified by the L matrix with linear approximations that can be calculated according to equation 8. Figure 2b shows the freely estimated parameters including variances, covariances, frequencies η, and damping coefficients ζ. In this model, $y(t)$ is a combination of two damped linear oscillators described in equations (17) & (18), allowing for stochastic variation $u(t)$, overall affine slope and intercept μ and β (not pictured), and measurement error $\epsilon(t)$. In 2b, it can be seen that variance due to acceleration of the long-term oscillator is subtracted from the variance due to acceleration of the short-term oscillator in accordance with equation 18. In principle, more timescales may be included to describe successively longer periods of regulatory response, but the width of the data embedding window becomes multiplicatively larger for each additional scale.

$$\ddot{x}_L(t) = \eta_L[x_L(t) - \mu] + \zeta_L \dot{x}_L(t) \tag{17}$$

$$\ddot{x}_S(t) = \eta_S[x_S(t) - \ddot{x}_L(t)] + \zeta_S \dot{x}_S(t) + u(t) \tag{18}$$

$$y(t) = \mu + \beta t + x_S(t) + x_L(t) + \epsilon(t) \tag{19}$$

For this example model with two timescales, italicized subscripts L and S denote the long and short timescales, defined over two embedding dimensions D_L and D_S. The L matrix for this model differs from the basic LDE in that it includes the basic L matrix (8) as $K = D_L/D_S$ consecutive block submatrices $\mathrm{L}_{S,k}, k \in \{1, 2, ..., K\}$ organized along its diagonal. These submatrices model K equivalent subsets of the total embedding window. Parameters in the corresponding S_k and A_k submatrices are constrained to be invariant across subsets. The fixed paths for the long-term dynamics are determined by the same algebra but span the entire time-embedding window. For instance, the matrix L_L for a total time-embedding dimension $D_L = 12$ on unit time and occasion intervals $\tau = \Delta t = 1$ is shown in equation (21), and incorporated into the L matrix for AER as shown in (20):

$$\mathrm{L} = \left[\begin{array}{ccc|c} \mathrm{L}_{S,1} & & 0 & \\ & \ddots & & \\ & \mathrm{L}_{S,k} & & \mathrm{L}_L \\ 0 & & \ddots & \\ & & \mathrm{L}_{S,K} & \end{array}\right] \tag{20}$$

$$\mathrm{L}_L = \begin{array}{c} \\ y_{t+l(1)} \\ y_{t+l(2)} \\ y_{t+l(3)} \\ y_{t+l(4)} \\ y_{t+l(5)} \\ y_{t+l(6)} \\ y_{t+l(7)} \\ y_{t+l(8)} \\ y_{t+l(9)} \\ y_{t+l(10)} \\ y_{t+l(11)} \\ y_{t+l(12)} \end{array} \begin{array}{c} \begin{array}{ccc} x_L & \dot{x}_L & \ddot{x}_L \end{array} \\ \begin{bmatrix} 1 & l(1) & l(1)^2/2 \\ 1 & l(2) & l(2)^2/2 \\ 1 & l(3) & l(3)^2/2 \\ 1 & l(4) & l(4)^2/2 \\ 1 & l(5) & l(5)^2/2 \\ 1 & l(6) & l(6)^2/2 \\ 1 & l(7) & l(7)^2/2 \\ 1 & l(8) & l(8)^2/2 \\ 1 & l(9) & l(9)^2/2 \\ 1 & l(10) & l(10)^2/2 \\ 1 & l(11) & l(11)^2/2 \\ 1 & l(12) & l(12)^2/2 \end{bmatrix} \end{array} = \begin{bmatrix} 1 & -5.5 & 15.125 \\ 1 & -4.5 & 10.125 \\ 1 & -3.5 & 6.125 \\ 1 & -2.5 & 3.125 \\ 1 & -1.5 & 1.125 \\ 1 & -0.5 & 0.125 \\ 1 & 0.5 & 0.125 \\ 1 & 1.5 & 1.125 \\ 1 & 2.5 & 3.125 \\ 1 & 3.5 & 6.125 \\ 1 & 4.5 & 10.125 \\ 1 & 5.5 & 15.125 \end{bmatrix} \tag{21}$$

(a) Fixed derivative estimation paths specified by the L matrix (equation 20)

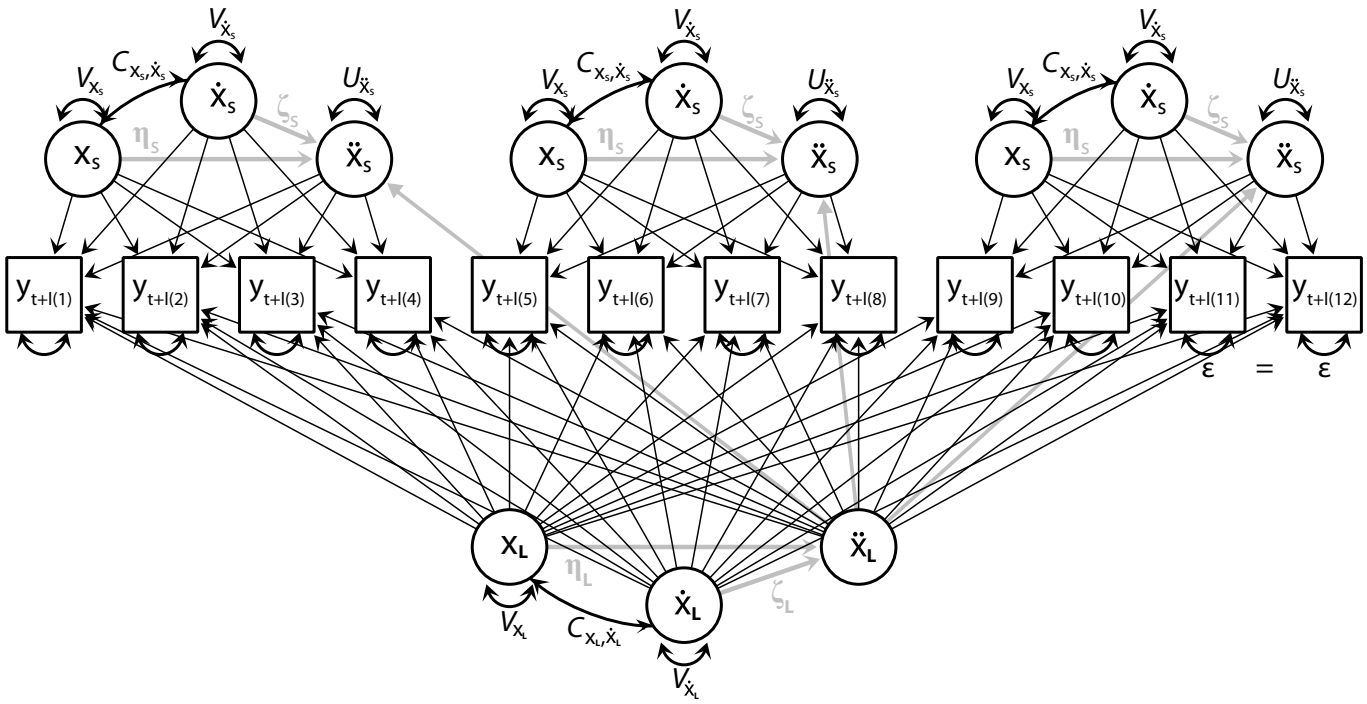

(b) Freely estimated parameters specified by the A matrix (equation 22)

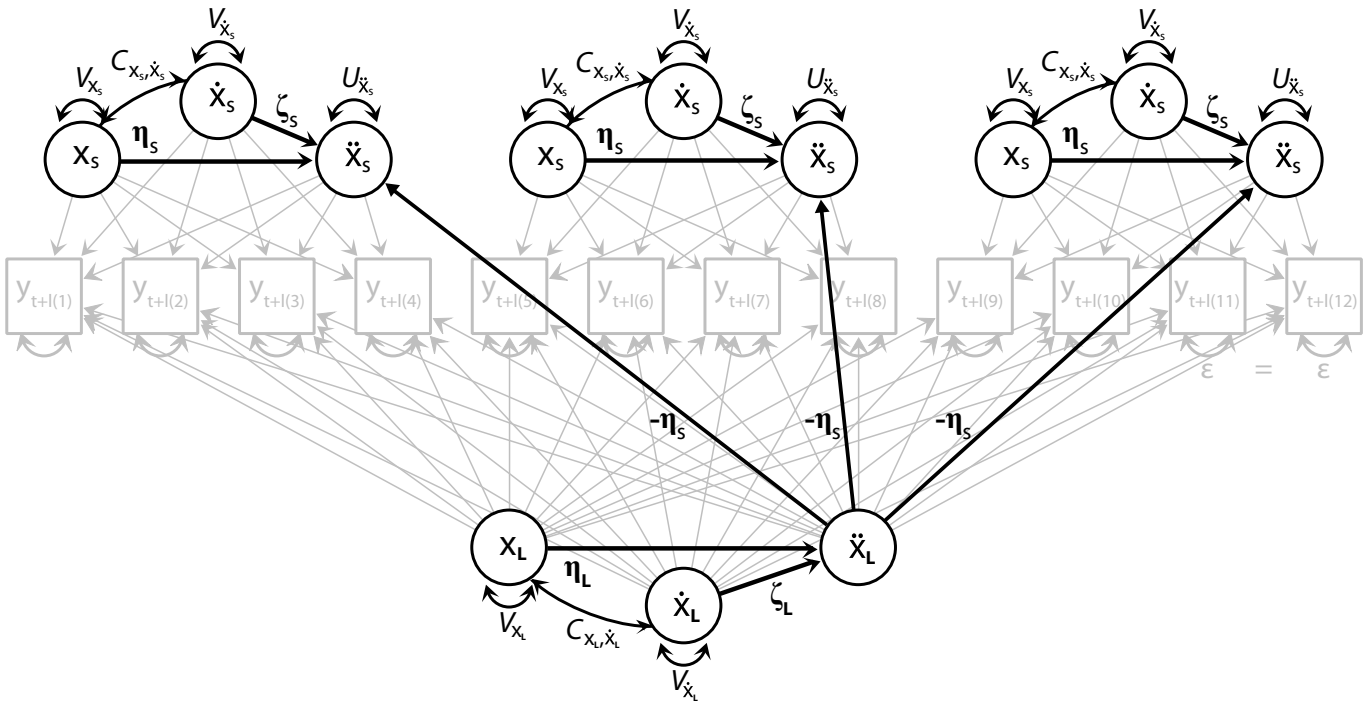

Figure 2: Adaptive Equilibrium Regulation as two nested 2nd-order models at different timescales.

Similarly, the A matrix for AER includes submatrix (16) organized along the diagonal, with the last submatrix containing the long-term dynamic coefficients. According to equation (18), we estimate the paths from the long to short-term acceleration as $-\eta_S$.

$$\mathrm{A} = \left[\begin{array}{ccc|c} \mathrm{A}_{S,1} & & \mathbf{0} & \\ & \ddots & & \\ & \mathrm{A}_{S,k} & & \mathbf{A}_L \\ & & \ddots & \\ \mathbf{0} & & \mathrm{A}_{S,K} & \end{array}\right] \quad \mathrm{A}_L = \begin{array}{c} \\ x_{S,1} \\ \dot{x}_{S,1} \\ \ddot{x}_{S,1} \\ \vdots \\ x_{S,k} \\ \dot{x}_{S,k} \\ \ddot{x}_{S,k} \\ \vdots \\ x_{S,K} \\ \dot{x}_{S,K} \\ \ddot{x}_{S,K} \\ x_L \\ \dot{x}_L \\ \ddot{x}_L \end{array} \begin{array}{c} \begin{array}{ccc} x_L & \dot{x}_L & \ddot{x}_L \end{array} \\ \left[\begin{array}{ccc} 0 & 0 & 0 \\ 0 & 0 & 0 \\ 0 & 0 & -\eta_S \\ \vdots & \vdots & \vdots \\ 0 & 0 & 0 \\ 0 & 0 & 0 \\ 0 & 0 & -\eta_S \\ \vdots & \vdots & \vdots \\ 0 & 0 & 0 \\ 0 & 0 & 0 \\ 0 & 0 & -\eta_S \\ 0 & 0 & 0 \\ 0 & 0 & 0 \\ \eta_L & \zeta_L & 0 \end{array}\right] \end{array} \tag{22}$$

The S matrix again follows the same structure with a unique block matrix for the long-term derivative variances and covariance. $U\ddot{x}$ is excluded from this matrix because stochastic variation is accounted for in the short-term model.

$$\mathrm{S} = \left[\begin{array}{ccc|c} \mathrm{S}_{S,1} & & \mathbf{0} & \\ & \ddots & & \\ & \mathrm{S}_{S,k} & & \\ & & \ddots & \\ \mathbf{0} & & \mathrm{S}_{S,K} & \\ \hline & & & \mathrm{S}_L \end{array}\right] \quad \mathrm{S}_L = \begin{bmatrix} V_{x_L} & C_{x_L,\dot{x}_L} & 0 \\ C_{x_L,\dot{x}_L} & V_{\dot{x}_L} & 0 \\ 0 & 0 & 0 \end{bmatrix} \tag{23}$$

To date, no simulations or applications have been carried out to test the viability of models in which time-embedding windows are nested in this way. Specifically, it is unclear how the model will perform given different ratios of two timescales. For ratios close to 1:1, the respective dynamic parameters of each may confound one another. Simulations were carried out to examine parameter recovery for four timescale ratios. Second, the impact of each timescale ratio on robustness to measurement error was tested for four variances of superposed measurement noise.

Methods

Software

All scripts were written in R software environment, version 3.4.2 (R Core Team, 2017). Data series were simulated using R package deSolve (Soetaert et al., 2010), version 1.2. The R package OpenMx, version 2.7.16 (Neale et al., 2016), was used to specify and fit all models, with the default gradient descent optimizer set to NPSOL (Philip et al., 2001). OpenMx was chosen because it provides a transparent, open-source platform for structural equation modeling. To fit each model, `mxRun()` was used with two additional re-runs in case of non-convergence. OpenMx optimizer status codes indicating final model convergence were logged with simulation outputs.

Simulation Design

We aimed to examine the precision and accuracy of parameter estimates for four possible timescale ratios and long-to-short oscillation periods: 2:1, 3:1, 4:1, and 5:1; three signal-to-noise ratios: low (16:1), moderate (4:1), and high (1:1), and three sample sizes as occasions-per-person: 75, 150, and 300, altogether comprising a $4 \times 3 \times 3$ design. Data were generated and models fit for 250 iterations per condition.

Several unknown factors influence the statistical power to model differential equations, and no method of determining and incorporating all of these factors a priori has yet been developed. Important factors include: 1) Chosen embedding dimensions, 2) sample size, 3) signal-to-noise ratio, 4) number of complete cycles within the sample, 5) the percentage of informative variance as a consequence of the damping ratio and innovational outliers (IO).[4] For a sufficiently long series with

[4]Innovational outliers often go by other names including events, dynamic error outliers, jump discontinuities, or disturbances.

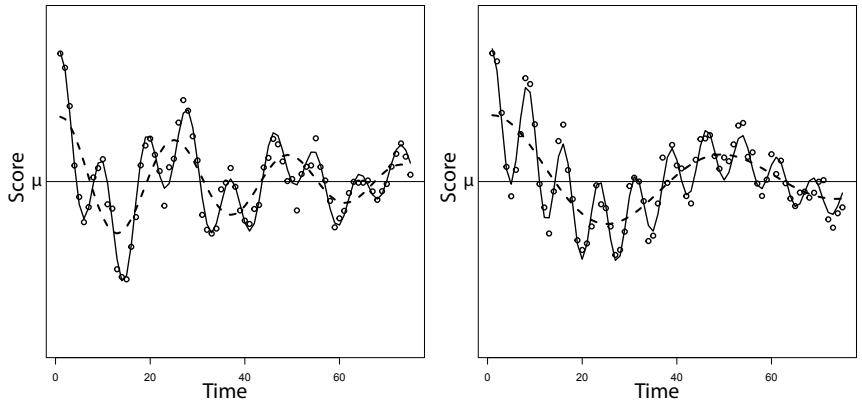

(a) Timescale Ratio 3:1 (b) Timescale Ratio 6:1

Figure 3: Simulated multi-timescale series with measurement error for two timescale ratios.

no IOs, a damped system will eventually sit at equilibrium and exhibit only as much variability as there is measurement error. IOs provide the necessary initial condition for a regulatory response pattern. Without the IO, additional data will not provide information about the dynamics under examination.

In reality, the occurrance of IOs may be theoretically important, related to measured covariates, or unknown. Algorithms have been developed to correct for outliers (Ih et al., 1988). Their application has yet to be shown with LDEs and data structured in a time-embedded format, though estimate biases due to such random processes have been demonstrated (Deboeck and Boker, 2010). For this reason, IOs were not included in the simulation process. Furthermore, dynamic error was not simulated and $U_{\ddot{x}}$ was constrained to 0. Instead, each component of the signal began with initial level = 1, and values of ζ were computed as a function of N so that the last peak of each simulated series would be half the amplitude of the first.

Timescale was defined as a function of corresponding values for D_L, η_L, ζ_L, and total occasions N. An explanation for how values for each of these conditions were chosen is subsequently described.

D_S First, a base value of $D_S = 4$ was chosen to balance minimal bias and robustness to measurement error when modeling relatively high frequency oscillations.

D_L The ratio of timescales was varied by confining the short-term frequency to a small range appropriate for $D_S = 4$, and simulating incrementally slower long-term oscillations. D_L was varied as multiples $2D_S$ through $5D_S$. It is also possible with overlapping D_S subsets to specify the model for non-integer timescale ratios.

η_S Boker et al. (2010) recommends choosing a value for D spanning at least half of the occasions per period, as time dependence tends to diminish for further lags. Selecting a dimension too large may bias η estimates toward slower frequencies due to excessive smoothing of the latent level x. If our simulation represents ideal specification of the model with respect to the natural frequency of the series, then $D_S = \lambda_S/2$, where λ_S is the number of occasions per period of short-term oscillation. Hence, η is calculated as follows:

$$\lambda_S = 2D_S = 8 \qquad \eta_S \approx -\left(\frac{2\pi}{\lambda_S}\right)^2 \approx -0.6168503 \tag{24}$$

According to this procedure, each value of η_L would represent a harmonic frequency of η_S. For small timescale ratios, harmonic frequencies will have unusually correlated derivatives which may not be representative of the general case. To avoid only testing harmonic ratios between η_S and η_L, uniform random variation $U(-.1, .1)$ was added to η_S at each iteration, giving a default range of $U(-0.5168, -0.7168)$. This range of values allows between approximately 7.42 to 8.74 occasions per short term cycle and is not expected to have a large impact on the variance or bias of estimates divided by their true values, as will be discussed later.

η_L Similarly to η_S, η_L was calculated as a function of $\lambda_L = 2D_L$ using equation (2), but no random variation was added.

ζ_S, ζ_L To ensure that each simulated series ends with half of its initial amplitude, we computed ζ_S and ζ_L as functions of the total occasions N, η_S, and η_L. This was done according to equations (3), with peak amplitude ratio $x1/x0$ derived as:

$$\Delta = \frac{1}{2^{\frac{\lambda}{N}}} \tag{25}$$

N We chose total number of occasions 75, 150, and 300 to: 1) Allow a sufficient number of oscillatory periods up to the maximum timescale tested; 2) Reflect common, realistic, and attainable sample sizes in current psychological research; 3) Provide reasonable statistical power to test for model misspecification.

Each simulated series was generated using the following steps: 1) A differential equation with the simulation parameters and initial conditions was numerically integrated over time for each component of the signal. Initial conditions were both fixed to levels of 1 and slopes of 0. 2) The two resulting vectors were then summed to give a series with two oscillatory components, seen as the dashed and solid curves in Figure 3. Subfigures 3a and 3b illustrate how timescale was defined by different values of long-term frequency, η_L (dashed curve). 3) The summed series was then standardized to z-scores and a vector of normal, independent, and identically distributed random noise was added. An example of the final simulated values are shown by the points along each series in Figure 3.

The models were specified as described above and shown in Figure 2, according to a two-timescale, nested 2nd-order Latent Differential Equation, then fit to data using maximum likelihood estimation with the OpenMx commands `mxExpectationNormal()` and `mxFitFunctionML()`, assuming multivariate residual normality. Both η parameters were constrained to be negative, non-zero, and greater than the Nyquist frequency, ($-\pi^2 < \eta < 0$), that is, the maximum frequency that can be correctly estimated given the sampling rate. Frequencies above this boundary would be aliased as lower frequencies. Because data were generated to be mean stationary with no stochastic variation, the overall slope and short-term stochastic variation $U_{\dot{x}_S}$ were constrained to zero, substantially improving model runtime and convergence. No constraints were placed on the estimation of either ζ.

Analyses

All values of η were converted to occasions-per-period according to equation (2), and values of ζ were converted to rates of amplitude decrement, i.e. the ratios of consecutive peaks x_0/x_1 as calculated in equation (3). Converted estimates were divided by true values, and the ratio medians and standard deviations were computed. This way, each result in Table 2 can be interpreted as the median error of estimated period and amplitude decrement. OpenMx status codes 5 or 6 indicated iterations with a non-positive definite Hessian or failure of convergence. Iterations with these results were excluded from the analysis because they were likely to contain extreme parameter and standard error estimate outliers, particularly for each ζ where no upper or lower boundaries were used.

Affect Data

Measures

To demonstrate how the multi-timescale LDE can be applied to real data, two individuals were selected from an experience sampling data set of positive affect. Adult participants drawn from the community rated current positive affect for twenty days on four indicators: happy, pleased, joyful, and enjoyment. Each scale ranged from 0 (none) to 6 (extreme) (Diener et al., 1985). Person A provided from 6 to 10 ratings per day, 7.6 on average (total $N_A = 151$). Person B provided between 2 and 9 ratings per day, with 6.1 on average (total $N_B = 103$). Sampling intervals were treated as uniform. For more information about this data set, see (Moskowitz and Zuroff, 2004).

Indicators of positive affect were designed to reflect a single underlying axis. It is common practice to sum the scores across indicators for each occasion into a unified measure. For this study, we use an alternative approach, Singular-Value Decomposition (SVD), in which each indicator is weighted by importance to the common, underlying factor. SVD can be stated as $\mathrm{Y}=\mathrm{U}\Sigma\mathrm{V}^T$, where U is an $m \times n$ matrix of the eigenvectors of YY^T, V is an $n \times n$ matrix of the eigenvectors of $\mathrm{Y}^T\mathrm{Y}$, and Σ contains the eigenvalues of both U and V ranking the magnitude of each component dimension. By performing this operation on the raw positive affect indicators, the first column of U can be used as principal component scores along the underlying dimension of positive affect.

The use of principal component scoring accords with the theoretical dimensions for which the indicators were designed, and confers four main advantages over sum scores. 1) Indicators are weighted according to their representativeness of the underlying construct; 2) Scores can be weighted for each participant to adjust for variation in principal component structure. 3) Measurement error and related sources of variance unique to each indicator are relegated to the lower-ranked components and discarded. 4) For time series data, underlying factors may result in time-dependence within and between indicators. Time dependence can be included by time-embedding the indicators before computing the SVD. For the present study, 2 consecutive lags (Y_{t-1}, Y_{t-2}) were included for each indicator. Eigenvalues estimated for each individual consistently showed only a single major underlying component for positive affect; only the first column of U was used in subsequent analyses.

Preliminary Analyses

Descriptive measures were used to determine the time-dependent structure of each series to inform the specification of each embedding dimension for each individual. Spectral analysis provides one simple method, using a Fast Fourier Transform to decompose the series into its most prominent component frequencies. This was done for all participants in the study. Two individuals were selected for having two prominent oscillation periods with a ratio of at least 3:1. The Periodograms in Figure 4 show the coefficients of each frequency, for each individual's series. The two frequencies with the largest coefficients

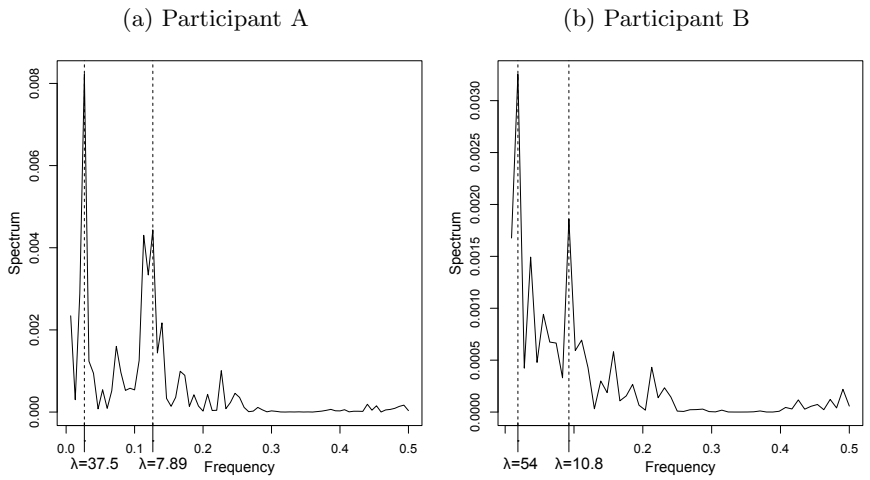

Figure 4: Periodograms for two individuals

are marked with the dotted line. Occasions-per-period λ are calculated from the frequency values and shown below the axis, with participant A showing slightly more than a 4:1 timescale ratio, and participant B at 5:1.

Model Specification

In accordance with the period (λ) of each major frequency, a model for participant A was specified at $D_S = 4, D_L = 16$, and for participant B, $D_S = 5, D_L = 25$. Stochastic variation $U_{\ddot{x}}$ and overall slope and intercept were all freely estimated. Final model comparisons examined the significance and impact upon estimates of excluding short term dynamics, long term dynamics, and stochastic variation using the likelihood-ratio test.

Results

Simulation

Rates of model non-convergence for each condition are shown in Table 1. The greatest contributor to non-convergence was timescale ratio, with the smallest, 2:1 consistently failing for approximately 20-50% of iterations. With high measurement error, timescale ratio 3:1 also showed minor rates of failure. All timescales exhibited some non-convergence or non-convexity due to the combination of high measurement error and low sample size. For the remainder of conditions, generally 100% of the iterations converged when oscillation periods were sufficiently distinct.

Table 1: Non-Convergence Rates by timescale ratio (TSR), number of occasions (N), and measurement error (ϵ)

ϵ		.00625			.25			1		
N		75	150	300	75	150	300	75	150	300
TSR	2:1	0.29	0.37	0.63	0.24	0.26	0.46	0.20	0.19	0.28
	3:1	0.00	0.00	0.00	0.01	0.00	0.00	0.11	0.03	0.02
	4:1	0.00	0.00	0.00	0.00	0.00	0.00	0.05	0.00	0.00
	5:1	0.00	0.00	0.00	0.00	0.00	0.00	0.03	0.00	0.00

Ratios of estimated to true oscillation period and amplitude decrement for short-term and long timescales are shown in Figures 5 through 7, with medians in Table 2 and standard deviations in Table 3. The dotted line in each plot represents equality of the estimate with its true value, and plots are subset by timescale ratio and total occasions.

For conditions with good model convergence rates, the estimates of short term period showed consistent, upward bias, averaging around 1.1× the true period, with long-term period only slightly higher at 1.12× the true values. Standard deviations for each were also small, around .01 to .02 and roughly the same for both short and long-term frequency. Short-term damping exhibited almost no appreciable bias and greater precision than long-term damping. All estimates reduced precision by half per each four-fold increase in measurement error and doubled in precision per each doubling of sample size.

For conditions with high rates of non-convergence, results tended toward uninterpretable extremes. Cells marked $> 1e3$ in Tables 2 and 3 contained extreme values on the order of $> 10^3$ even after non-convergent iterations were excluded.[5] For

[5]See Appendix 1.2 for unconverted estimate ratios

Table 2: Median period and amplitude decrement estimate/true ratios by timescale ratio (TSR), number of occasions (N), and measurement error (ϵ)

(a) $\hat{\eta}_L/\eta_L$ (as oscillation period)

ϵ		.00625			.25			1		
N		75	150	300	75	150	300	75	150	300
TSR	2:1	0.845	0.854	0.857	0.801	0.803	0.806	0.753	0.759	0.762
	3:1	1.131	1.128	1.128	1.147	1.142	1.144	1.023	1.076	1.104
	4:1	1.100	1.099	1.096	1.094	1.089	1.089	1.056	1.060	1.071
	5:1	1.086	1.091	1.092	1.078	1.088	1.091	1.054	1.067	1.076

(b) $\hat{\zeta}_L/\zeta_L$ (as amplitude decrement)

ϵ		.00625			.25			1		
N		75	150	300	75	150	300	75	150	300
TSR	2:1	0.671	0.839	0.940	0.631	0.829	0.915	0.787	0.888	0.952
	3:1	1.011	1.005	1.003	1.005	1.002	1.006	1.036	0.988	1.001
	4:1	0.938	0.962	0.985	0.888	0.944	0.977	0.937	0.949	0.967
	5:1	0.959	0.995	1.002	0.931	0.992	0.998	0.911	0.967	0.998

(c) $\hat{\eta}_S/\eta_S$ (as oscillation period)

ϵ		.00625			.25			1		
N		75	150	300	75	150	300	75	150	300
TSR	2:1	0.321	1.195	1.214	1.169	1.178	1.185	1.149	1.229	1.258
	3:1	1.126	1.126	1.124	1.168	1.172	1.166	1.235	1.250	1.256
	4:1	1.103	1.102	1.100	1.120	1.120	1.119	1.129	1.141	1.139
	5:1	1.103	1.104	1.102	1.117	1.120	1.120	1.118	1.133	1.137

(d) $\hat{\zeta}_S/\zeta_S$ (as amplitude decrement)

ϵ		.00625			.25			1		
N		75	150	300	75	150	300	75	150	300
TSR	2:1	$> 1e3$	0.609	0.795	14.638	0.802	0.837	1.401	1.312	1.167
	3:1	0.990	0.998	0.999	0.977	0.995	0.997	0.955	0.986	0.991
	4:1	1.000	1.000	1.001	0.992	0.997	0.999	0.989	1.000	0.997
	5:1	0.987	0.996	0.998	0.989	0.995	0.998	0.992	0.999	0.999

Table 3: Standard deviations of period and amplitude decrement estimate/true ratios by timescale ratio (TSR), number of occasions (N), and measurement error (ϵ)

(a) $\hat{s}\eta_L$ (as oscillation period)

ϵ		.00625			.25			1		
N		75	150	300	75	150	300	75	150	300
TSR	2:1	0.017	0.009	0.005	0.064	0.014	0.008	0.240	0.030	0.020
	3:1	0.045	0.018	0.014	0.085	0.037	0.024	0.759	0.164	0.085
	4:1	0.041	0.010	0.007	0.034	0.021	0.011	0.133	0.052	0.034
	5:1	0.024	0.009	0.006	0.046	0.019	0.012	0.146	0.066	0.036

(b) $\hat{s}\zeta_L$ (as amplitude decrement)

ϵ		.00625			.25			1		
N		75	150	300	75	150	300	75	150	300
TSR	2:1	0.125	0.075	0.030	0.201	0.128	0.075	0.296	0.161	0.076
	3:1	1.192	0.044	0.021	0.186	0.079	0.037	$> 1e3$	$> 1e3$	0.092
	4:1	0.277	0.044	0.021	0.179	0.087	0.040	113.581	0.165	0.080
	5:1	0.124	0.048	0.025	0.215	0.101	0.050	0.713	0.197	0.100

(c) $\hat{s}\eta_S$ (as oscillation period)

ϵ		.00625			.25			1		
N		75	150	300	75	150	300	75	150	300
TSR	2:1	0.406	0.396	0.122	0.662	0.614	0.429	0.490	0.462	0.289
	3:1	0.028	0.013	0.008	0.053	0.037	0.022	0.180	0.086	0.060
	4:1	0.026	0.010	0.007	0.045	0.031	0.018	0.189	0.093	0.055
	5:1	0.015	0.009	0.006	0.041	0.025	0.020	1.952	0.092	0.047

(d) $\hat{s}\zeta_S$ (as amplitude decrement)

ϵ		.00625			.25			1		
N		75	150	300	75	150	300	75	150	300
TSR	2:1	$> 1e3$	$> 1e3$	$> 1e3$	$> 1e3$	$> 1e3$	$> 1e3$	$> 1e3$	$> 1e3$	$> 1e3$
	3:1	0.028	0.013	0.006	0.065	0.027	0.013	0.251	0.094	0.043
	4:1	0.028	0.013	0.006	0.064	0.027	0.011	0.237	0.089	0.036
	5:1	0.027	0.012	0.005	0.056	0.025	0.012	0.234	0.086	0.032

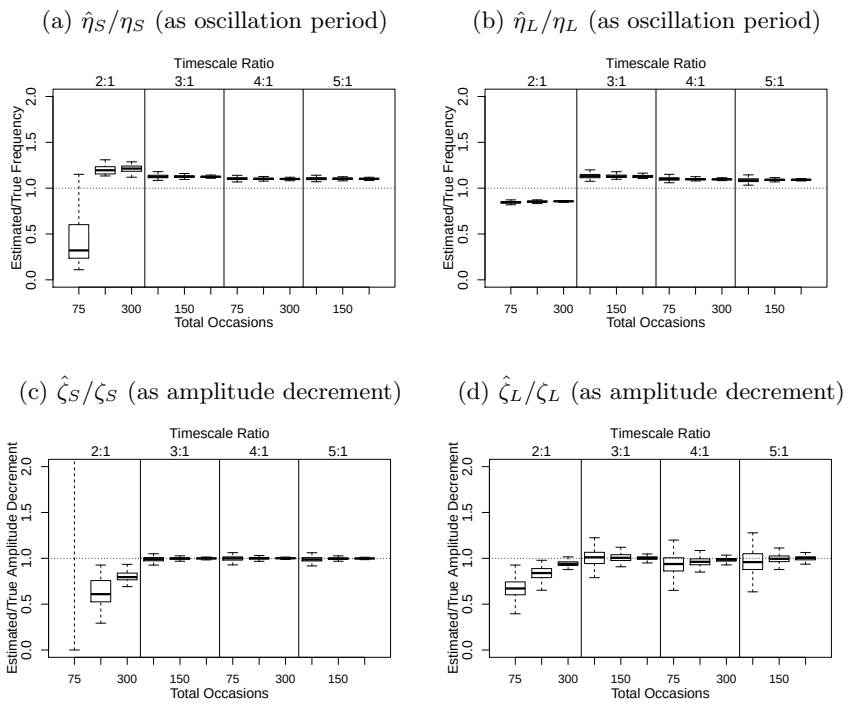

Figure 5: Ratios of converted parameter estimates to true values for low measurement error variance: ϵ=.00625

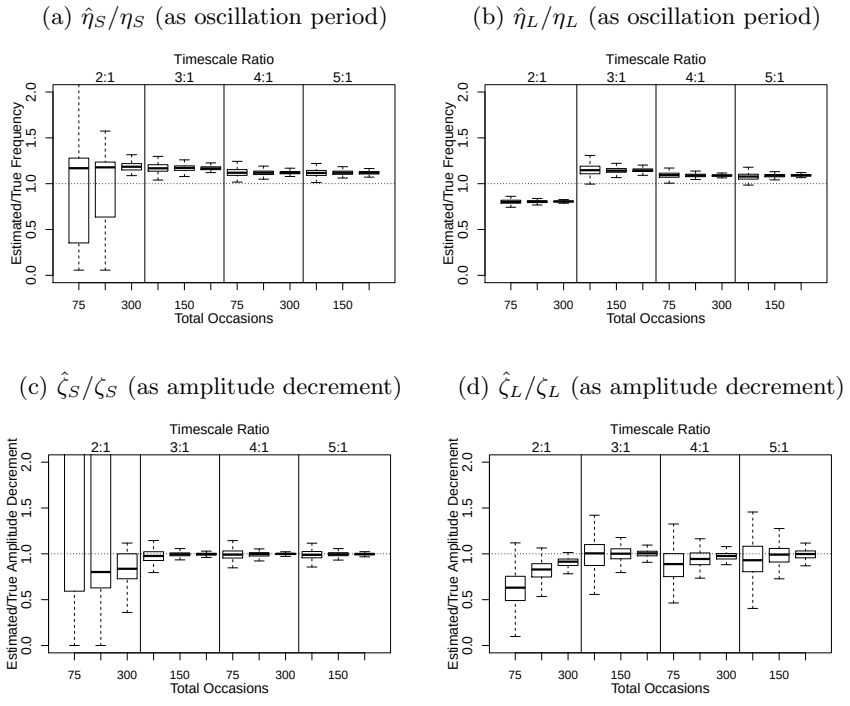

Figure 6: Ratios of converted parameter estimates to true values for moderate measurement error variance: ϵ=.25

a timescale ratio of 2:1, long-term period tended to bias toward fewer occasions per cycle with $\hat{\eta}_L$ closer to $\hat{\eta}_S$. Short-term damping showed irregular patterns of bias, while long-term amplitude decrement tended toward .6 to .8 of the true rate. Long-term damping also exhibited unpredictable and extreme error at combinations of high measurement error, low timescale ratio, and low sample size.

Tables 7, 8, and 9 in Appendix 1.2 show the medians of unconverted parameter estimate bias ratios, standard deviations, and parametric standard errors estimated by maximum likelihood. For conditions with good convergence rates, estimated parametric standard errors tended to be higher than the standard deviations by a factor of 2 or more. This relationship held

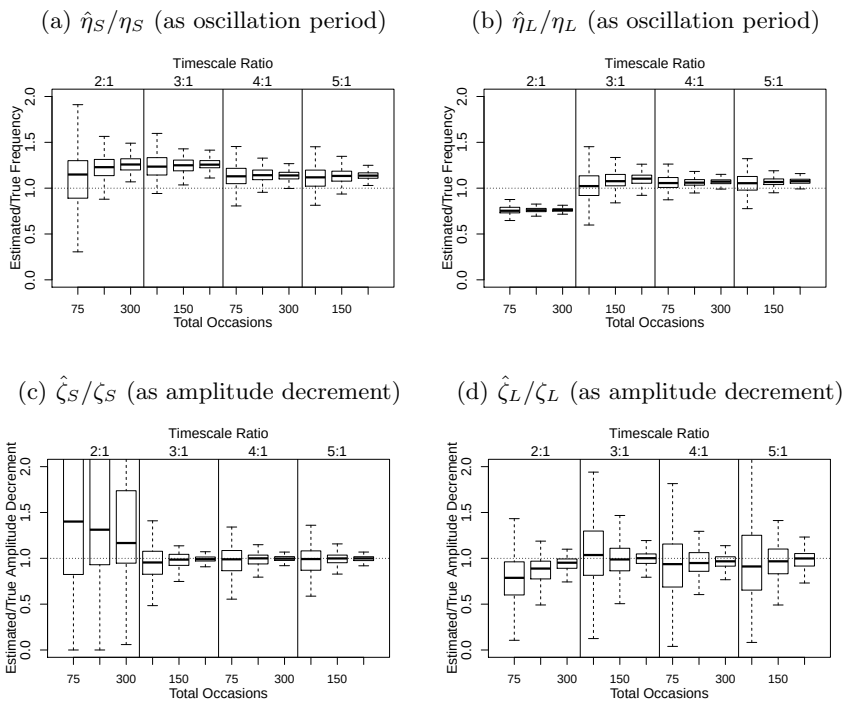

Figure 7: Ratios of converted parameter estimates to true values for high measurement error variance: ϵ=1

true even for the extreme variances produced by problematic conditions such as the smallest timescale ratio.

Affect

Base models converged without error for both individuals tested. Fit statistics are shown in Tables 4a and 5a. Fit comparisons between the base and submodel are given by the -2Log-Likelihood (-2LL) and Akaike Information Criterion (AIC) (Akaike, 1974), with lower values of either indicating better fit. Significance was defined at $\alpha = .05$, and likelihood-ratio tests were used to compare each submodel. The total number of estimated parameters (ep) is listed as well. Parameter estimates are shown in Tables 4b and 5b. For participant A, dynamic error, or stochastic variation, could be constrained to 0 without loss of the goodness of fit estimate or change in parameter estimates. Participant B showed significant dynamic error; constraining dynamic error to 0 resulted in slight changes to dynamic estimates and increased the estimated measurement error variance. For both individuals, both long and short term dynamics were statistically significant. Tables 4a and 5a show how the estimates for either timescale differed when the other timescale was excluded from the model.

Table 4: Results for participant A

(a) Model Fit

Model	ep	minus2LL	df	AIC	diffLL	diffdf	p
	14	4408.43	2130	148.43			
No Dyn.Err.	13	4408.90	2131	146.90	0.47	1	0.49
No Long	9	4576.19	2135	306.19	167.76	5	$< 10^{-3}$
No Short	8	5587.70	2136	1315.70	1179.26	6	$< 10^{-3}$

(b) Dynamic Estimates

	$\hat{\eta}_S$	$\hat{\zeta}_S$	$\hat{\eta}_L$	$\hat{\zeta}_L$	$\hat{\epsilon}$
Base	-0.5062	-0.0015	-0.0181	0.0032	0.1025
No Dyn.Err.	-0.5046	-0.0016	-0.0180	0.0032	0.1051
No Long	-0.3514	0.0021			0.1025
No Short			-0.0206	0.0000	0.1025

Table 5: Results for participant B

(a) Model Fit

Model	ep	minus2LL	df	AIC	diffLL	diffdf	p
	14	4023.61	1911	201.61			
No Dyn.Err.	13	4086.46	1912	262.46	62.85	1	$< 10^{-3}$
No Long	9	4101.33	1916	269.33	77.72	5	$< 10^{-3}$
No Short	8	4938.53	1917	1104.53	914.92	6	$< 10^{-3}$

(b) Dynamic Estimates

	$\hat{\eta}_S$	$\hat{\zeta}_S$	$\hat{\eta}_L$	$\hat{\zeta}_L$	$\hat{\epsilon}$
Base	-0.2980	-0.0241	-0.0132	-0.0228	0.1454
No Dyn.Err.	-0.2849	-0.0291	-0.0130	-0.0215	0.1839
No Long	-0.1980	-0.0295			0.1454
No Short			-0.0134	-0.0275	0.1454

Discussion

Simulations

The simulations demonstrate that the model is capable of reliable and precise estimation of frequency and damping dynamics on two timescales as long as they are characterized by sufficiently distinct oscillatory periods. Frequencies were somewhat recoverable even at the smallest ratios tested. In these cases, both frequency estimates were biased toward an intermediate value, but damping was entirely irretrievable. If measurement error is low, both damping and frequency could be recovered at ratios as low as 3:1.

The model also exhibited reasonable robustness to measurement error, with better results for more distinct oscillation periods and higher sample sizes. Because each signal was a standardized combination of two component signals, the maximum ratio of measurement error added with regard to each component separately was 2:1. The simulations also demonstrate a proportional increase in precision with sample size. Higher precision of short-term estimates, especially damping, corresponded with greater numbers of complete cycles across the sample. This is also evidenced by the slight increase in the standard deviation of long-term damping at timescale ratio 5:1 with only 75 total occasions, a condition reflecting the smallest number of complete long-term cycles within the sample.

The small, consistent bias toward lower frequencies in both long and short term estimates reflects an underlying limitation to estimating derivatives via discrete, 2nd-order polynomial approximations. Boker et al. (2010) demonstrated that increasing the embedding dimension results in lower estimates of frequency, while increasing the order of derivatives to be estimated partly mitigates the bias. Deboeck and Boker (2011) provide an analysis of parameter bias in Local Linear Approximation and a model-based method of correction using time-embedding windows of multiple widths per model fit. With OpenMx, the command `mxSE()` can be used obtain standard error estimates for the corrected parameter estimates. For comparing individuals within a random effects, multilevel framework, consistent parameter bias may only have a small impact on the between-persons covariance structure of individual parameters. If the intent is to forecast using model estimates, biased frequency estimates will result in a much quicker decay in the accuracy of a prediction over time, and it is advisable to use a method of correction such as Deboeck's.

Affect Data

The application of the model to positive affect demonstrates individual differences in dynamics and stochastic variation. Model fit comparisons demonstrate oscillations in affect at multiple timescales; failing to account for either impacted model fit and resulting parameter estimates. Long-term estimates incurred less bias when excluding short-term oscillations than vice versa. The periodograms in Figures 4a and 4b suggest that this is because the long-term amplitudes were much higher for both individuals.

To graphically examine the results of each model, ordinary differential equations with model estimates as coefficients were numerically integrated and fit via optimization to the data series. The solutions are compared in Figure 8. These deterministic trajectories align to the data well for short periods of time, but the phase alignment for both long and short oscillations can be seen to decay further along the series. The misalignment is likely due to dynamic error and innovational outliers leading to phase drift in the data. Unlike the strictly deterministic trajectories shown, real processes will not oscillate with perfect regularity. These figures demonstrate the need for compatible methods of accounting for innovational outliers to improve the accuracy of estimates, particularly if such trajectories will be used to forecast future states. For more general purposes, the oscillation periods at both timescales give a static description of each individual's dynamic tendency. With sufficient data on an individual, it seems likely that these methods will increasingly capture intrinsic traits of interest to psychology and psychiatry.

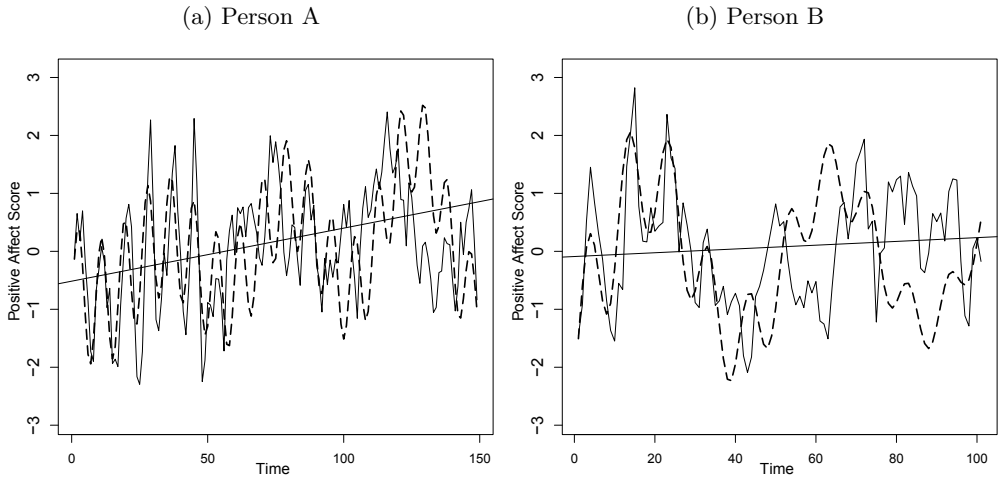

Figure 8: Numerically integrated trajectories (dashed curve) aligned to raw data (solid lines); overall equilibrium nonstationarity is shown by the straight lines.

Limitations

An unusual aspect of time-embedding on multiple dimensions is that the short embedding window is nested within the long embedding window in consecutive repetitions, as can be seen from Figure 2, and each repetition of the model is constrained to estimate the same parameters as its duplicates, that is, each models exactly the same dynamic behavior but at different occasions. This means that for $D_L = 3D_S$, the influence of each occasion on the short-term model may be triplicated. Additional simulations were run to test for possible consequences of specifying models this way, and a summary of their results can be found in Appendix 1.1. In brief, redundant modeling does not appear to bias the estimates but slightly decreases estimated parametric standard errors. Furthermore, our results confirm the observations by von Oertzen and Boker (2010) that standard deviations of estimates will be lower than estimated due to the manner in which symmetrical time-embedding cancels out bias introduced by measurement error. As they have advised, bootstrapping standard errors should be considered for accurate estimates of precision in real applications. In practice, this would nullify the consequences of biased standard errors due to multiply embedding the data by simply rejecting the estimated parametric standard errors altogether.

One limitation of this study was that capacity to account for dynamic error was not tested in the simulations. Real behavioral or psychological data are likely to exhibit non-systematic random influence from unmeasured sources, the effects of which would be modeled as additional, normally distributed variance of the short-term second derivative. Innovational outliers have been demonstrated to bias the estimates of damping to zero or positive values, miserepresenting data as undamped or even amplifying (Deboeck and Boker, 2010). In modeling affect data for the current study, no method of detecting innovational outliers was used. Unsurprisingly, the estimates of damping for both individuals were small. Without a method of modeling or classifying innovations to the signal, the damping parameter ζ will be determined by the average change in amplitude across the whole series. If the variance of the series is stationary, damping will be estimated close to zero. It is incumbent upon researchers interested in the accurate estimation of damped systems to adopt a method of handling outliers either by removal (Ih et al., 1988), by including appropriate time-varying covariates of the second derivative, or by beginning a series of measures with an intervention of interest and controlling for exogenous influences on the response. Post-hoc, algorithmic strategies may be used to detect innovational outliers, and will be examined in future work.

We also did not simulate cases where the amplitudes of each component differed, though it is a likely that for many applications, long-term oscillations would represent only minor seasonal fluctuations in equilibrium relative to more volatile short term variation. For instance, if we are modeling affect, only severely disordered individuals would be expected to occupy the extremes of the emotional intensity scale for prolonged and invariant phases, whereas healthy individuals experience extremes commonly but briefly as the result of transient events. If a combination of seasonal patterns is suspected to contribute unequally to the total variability, the researcher must choose a sampling frequency and total number of occasions suitable to overcome the potential ratio of the faintest component signal to noise. Our simulations show that for an expected 1:2 ratio of signal-to-noise, it is advisable to measure at least 150 occasions with at least 8 occasions per shortest expected oscillation period and at least 24 occasions per long-term oscillation period. Below these, parameters may be recoverable but with increasing risk of confounding between frequencies and sensitivity to measurement error.

Further Extensions

It is possible to expand the model to include additional, higher scales of time by extending the same algebraic structure used here to relate only two. If more timescales are nested, the data resolution requirements and expectations of measurement error become stricter proportional to each additional timescale. This model may also be expanded to the multivariate case outlined by Hu et al. (2014) by cross-regressing derivatives between observed series on one or both timescales. This would allow variables, whether within or between persons, to exhibit influence on each other specific to timescale. Further simulations are warranted to determine how the increased complexity of multivariate linking would change the sensitivity to timescale ratio and the impact of timescale differences on the recovery of derivative coupling parameters.

While the proposed model represents a linear dynamical system, certain non-linear systems may be approximated through piecewise linear modeling (Storace and De Feo, 2004) or with moderated linear coefficients. For instance, neurons exhibit short bursts of action potentials, where high-amplitude, high-frequency oscillations occur at the peaks of slower, shallower fluctuations in membrane potential (Hindmarsh and Rose, 1984). Such non-linear dynamics could be approximated by moderating the parameters of a high-frequency oscillator by the derivatives of a gradual oscillation representing accumulated membrane potential.

The overlaid solution for Person A shown in Figure 8a depicts a damped, short-term system nested within an amplifying long-term system. Varying amplitudes of equilibrium oscillations between individuals may suggest that an underlying bifurcation occurs in this process. Furthermore, a damped or amplifying oscillation in equilibrium may give insight into the time frame over which such bifurcations occur in natural systems. While the analysis of non-linear systems is beyond the scope of this study, the approximation of non-linear systems by linear models remains an important possibility worth further development.

Conclusion

The proposed multi-timescale model of intra-individual dynamics has been demonstrated to recover frequency and damping parameters for multiple timescales with the caveat that for a ratio of frequencies below 3:1, damping behavior becomes more difficult to accurately discern, and frequency estimates will bias toward an intermediate value. For real data, the model showed individual differences in dynamic error and statistically significant dynamics at both timescales, supporting the hypothesis that such processes exist and must be modeled. Estimated dynamics were shown to accurately approximate patterns of individual change. For best results, the authors recommend additional steps to account for predictable biases due to derivative estimation and a strategy for accounting for outliers of dynamic error. The study outlines a general method of nesting latent differential equations at multiple scales of time that is suitable for the relatively sparse and noisy data typical of psychological studies.

Acknowledgments

The authors thank Drs. Joshua Pritikin, Steven Aggen, and Robert Kirkpatrick of Virginia Commonwealth University's Virginia Institute of Psychiatric and Behavioral Genetics for feedback on model development and OpenMx technical support. Collection of the affect data was supported by Social Sciences and Humanities Research Council of Canada and Fonds Pour la Formation de Chercheurs et lAide a‘ la Recherche du Quebec.

References

Akaike, H. (1974). A new look at the statistical model identification. *IEEE transactions on automatic control*, 19(6):716–723.

Barton, S. (1994). Chaos, self-organization, and psychology. *American Psychologist*, 49(1):5–14.

Boker, S., Deboeck, P. R., Schiller, C. E., and Keel, P. K. (2010). Generalized local linear approximation of derivatives from time series.

Boker, S., Neale, M., and Klump, K. (2014). A differential equations model for the ovarian hormone cycle. *Handbook of relational developmental systems: Emerging methods and concepts*.

Boker, S., Neale, M., and Rausch, J. (2004). Latent differential equation modeling with multivariate multi-occasion indicators. In *Recent developments on structural equation models*, pages 151–174. Springer.

Boker, S. M. (2002). Consequences of continuity: The hunt for intrinsic properties within parameters of dynamics in psychological processes. *Multivariate Behavioral Research*, 37(3):405–422.

Boker, S. M. (2012). Dynamical systems and differential equation models of change. In Cooper, H., Panter, A., Camic, P., Gonzalez, R., Long, D., and Sher, K., editors, *APA Handbook of Research Methods in Psychology*, pages 323–333. American Psychological Association, Washington, DC.

Boker, S. M. (2015). Adaptive Equilibrium Regulation: A Balancing Act in Two Timescales. *Journal for person-oriented research*, 1(1-2):99.

Boker, S. M. and Graham, J. (1998). A dynamical systems analysis of adolescent substance abuse. *Multivariate Behavioral Research*, 33(4):479–507.

Bollen, K. (1989). A.(1989). Structural equations with latent variables. *new york, ny: wiley. doi*, 10:9781118619179.

Chow, S.-M., Ram, N., Boker, S. M., Fujita, F., and Clore, G. (2005). Emotion as a thermostat: representing emotion regulation using a damped oscillator model. *Emotion*, 5(2):208.

Deboeck, P. R. and Boker, S. M. (2010). Modeling noisy data with differential equations using observed and expected matrices. *Psychometrika*, 75(3):420–437.

Deboeck, P. R. and Boker, S. M. (2011). Unbiased, smoothing-corrected estimation of oscillators in psychology. In Chow, S.-M., Ferrer, E., and Hsieh, F., editors, *Statistical methods for modeling human dynamics: An interdisciplinary dialogue*, pages 179–212. Taylor & Francis.

Diener, E., Larsen, R. J., Levine, S., and Emmons, R. A. (1985). Intensity and frequency: dimensions underlying positive and negative affect. *Journal of personality and social psychology*, 48(5):1253.

Ebner-Priemer, U. W., Houben, M., Santangelo, P., Kleindienst, N., Tuerlinckx, F., Oravecz, Z., Verleysen, G., Van Deun, K., Bohus, M., and Kuppens, P. (2015). Unraveling affective dysregulation in borderline personality disorder: A theoretical model and empirical evidence. *Journal of abnormal psychology*, 124(1):186.

Hindmarsh, J. L. and Rose, R. (1984). A model of neuronal bursting using three coupled first order differential equations. *Proceedings of the royal society of London B: biological sciences*, 221(1222):87–102.

Hu, Y., Boker, S., Neale, M., and Klump, K. L. (2014). Coupled latent differential equation with moderators: Simulation and application. *Psychological methods*, 19(1):56.

Ih, C., Tiao, G. C., and Chen, C. (1988). Estimation of time series parameters in the presence of outliers. *Technometrics*, 30(2):193.

McArdle, J. J. and McDonald, R. P. (1984). Some algebraic properties of the reticular action model for moment structures. *British Journal of Mathematical and Statistical Psychology*, 37(2):234–251.

Moskowitz, D. and Zuroff, D. C. (2004). Flux, pulse, and spin: dynamic additions to the personality lexicon. *Journal of personality and social psychology*, 86(6):880.

Neale, M. C., Hunter, M. D., Pritikin, J. N., Zahery, M., Brick, T. R., Kirkpatrick, R. M., Estabrook, R., Bates, T. C., Maes, H. H., and Boker, S. M. (2016). OpenMx 2.0: Extended structural equation and statistical modeling. *Psychometrika*, 81(2):535–549.

Oie, K. S., Kiemel, T., and Jeka, J. J. (2002). Multisensory fusion: simultaneous re-weighting of vision and touch for the control of human posture. *Cognitive Brain Research*, 14(1):164–176.

Oravecz, Z., Tuerlinckx, F., and Vandekerckhove, J. (2011). A hierarchical latent stochastic differential equation model for affective dynamics. *Psychological methods*, 16(4):468.

Philip, E., MURRAY, W., SAUNDERS, M. A., and Wright, M. H. (2001). USER'S GUIDE FOR NPSOL 5.0: A FORTRAN PACKAGE FOR NONLINEAR PROGRAMMING. Technical report, Technical report SOL 866.

R Core Team (2017). *R: A Language and Environment for Statistical Computing*. R Foundation for Statistical Computing, Vienna, Austria.

Rosenthal, N. E., Sack, D. A., Gillin, J. C., Lewy, A. J., Goodwin, F. K., Davenport, Y., Mueller, P. S., Newsome, D. A., and Wehr, T. A. (1984). Seasonal affective disorder: a description of the syndrome and preliminary findings with light therapy. *Archives of general psychiatry*, 41(1):72–80.

Smith, P. L. (2000). Stochastic dynamic models of response time and accuracy: A foundational primer. *Journal of mathematical psychology*, 44(3):408–463.

Soetaert, K., Petzoldt, T., and Setzer, R. W. (2010). Solving differential equations in R: package deSolve. *Journal of Statistical Software*, 33.

Storace, M. and De Feo, O. (2004). Piecewise-linear approximation of nonlinear dynamical systems. *IEEE Transactions on Circuits and Systems I: Regular Papers*, 51(4):830–842.

Tiberio, S. S. (2008). *The effects of misspecified measurement intervals in Multivariate Latent Differential Equation models.* University of Notre Dame.

Tuma, N. B. and Hannan, M. T. (1984). *Social Dynamics Models and Methods.* Elsevier.

von Oertzen, T. and Boker, S. M. (2010). Time delay embedding increases estimation precision of models of intraindividual variability. *Psychometrika*, 75(1):158–175.

Wei, W. W. (2006). *Time series analysis: univariate and multivariate methods.* Pearson Addison Wesley.

1 Appendix

1.1 Multiple Embedding Simulation

A simulation was run on a modification of the AER model in which the long-term dynamics were excluded, leaving only a multiply-embedded short-term model. 1000 iterations of data generation and model fit were performed with η and ζ parameters fixed to -.5 and -.3 respectively, signal-to-noise ratio to 8:1, initial conditions to a level of 1 and slope of 0, series length to 100 occasions, and mean slopes and intercepts both to 0. In this simulation, the number of repeated embeddings of the short-term model was tested for a biasing effect on the standard errors by using total embedding dimensions $D_L \in \{4, 8, 12, 16, 20\}$.

Table 6 shows that duplicating the short-term model alone has no impact on estimate bias or the standard error of the estimates obtained through simulation. The standard errors obtained by the Hessian through maximum likelihood estimation, however, appear to bias downward for both η and ζ as a result of any model duplication at all. The change is not linear, as this effect diminishes with repeated embeddings on larger dimensions D_L. It is also notable that the Hessian-based standard errors were approximately double the standard deviation of the estimates from simulation.

Table 6: Simulation Results: η, ζ recovery for multiply embedding D_S.

	η			ζ		
D_L/D_S	$\bar{X}$	$\hat{s}_{\bar{X}}$	$H\hat{s}_{\bar{X}}$	$\bar{X}$	$\hat{s}_{\bar{X}}$	$H\hat{s}_{\bar{X}}$
1	-0.4475	0.0128	0.0232	-0.2878	0.0124	0.0317
2	-0.4479	0.0106	0.0199	-0.2871	0.0116	0.0280
3	-0.4488	0.0110	0.0190	-0.2873	0.0113	0.0271
4	-0.4485	0.0118	0.0189	-0.2884	0.0115	0.0271
5	-0.4493	0.0120	0.0189	-0.2877	0.0112	0.0270

1.2 Unconverted Simulation Results

Table 7: Median unconverted η and ζ estimate/true ratios, by timescale ratio (TSR), total occasions (N), and measurement error (ϵ)

(a) $\hat{\eta}_L/\eta_L$

ϵ		.00625			.25			1		
N		75	150	300	75	150	300	75	150	300
TSR	2:1	1.4167	1.3747	1.3625	1.5762	1.5547	1.5424	1.7803	1.7462	1.7226
	3:1	0.7835	0.7858	0.7864	0.7590	0.7665	0.7637	0.9527	0.8661	0.8212
	4:1	0.8277	0.8294	0.8324	0.8416	0.8436	0.8432	0.8990	0.8912	0.8721
	5:1	0.8485	0.8405	0.8385	0.8613	0.8450	0.8403	0.9035	0.8781	0.8637

(b) $\hat{\zeta}_L/\zeta_L$

ϵ		.00625			.25			1		
N		75	150	300	75	150	300	75	150	300
TSR	2:1	2.7935	2.5695	2.1480	3.2614	2.8179	2.7140	2.4050	2.3788	2.1443
	3:1	0.8610	0.8645	0.8607	0.8746	0.8680	0.8303	0.8820	0.9524	0.9307
	4:1	1.0039	1.0286	1.0052	1.0923	1.0988	1.0627	1.0316	1.0986	1.1410
	5:1	0.9709	0.9277	0.9035	1.0072	0.9489	0.9289	1.0814	1.0330	0.9336

(c) $\hat{\eta}_S/\eta_S$

ϵ		.00625			.25			1		
N		75	150	300	75	150	300	75	150	300
TSR	2:1	0.8593	0.7101	0.6793	0.7634	0.7229	0.7112	0.7052	0.6635	0.6375
	3:1	0.7892	0.7883	0.7908	0.7334	0.7276	0.7352	0.6522	0.6405	0.6335
	4:1	0.8212	0.8230	0.8259	0.7979	0.7973	0.7985	0.7839	0.7681	0.7712
	5:1	0.8222	0.8207	0.8231	0.8009	0.7977	0.7974	0.8016	0.7790	0.7740

(d) $\hat{\zeta}_S/\zeta_S$

ϵ		.00625			.25			1		
N		75	150	300	75	150	300	75	150	300
TSR	2:1	-138.58	6.3448	5.9021	-14.724	3.3630	5.0072	-1.0294	-2.1436	-2.6408
	3:1	0.9537	0.9197	0.9198	0.9774	0.9247	0.9258	1.0553	0.9580	1.0248
	4:1	0.9103	0.9008	0.8897	0.9335	0.9328	0.9131	0.9094	0.8790	0.9308
	5:1	0.9854	0.9525	0.9489	0.9473	0.9498	0.9483	0.9829	0.8969	0.8876

Table 8: Standard deviations of unconverted η and ζ estimate/true ratios, by timescale ratio (TSR), total occasions (N), and measurement error (ϵ)

(a) $\hat{s}$ of η_L

ϵ		.00625			.25			1		
N		75	150	300	75	150	300	75	150	300
TSR	2:1	0.0062	0.0045	0.0026	0.0187	0.0079	0.0047	0.0480	0.0202	0.0136
	3:1	0.0112	0.0017	0.0013	0.0267	0.0033	0.0022	0.1017	0.1326	0.0108
	4:1	0.0070	0.0006	0.0004	0.0020	0.0012	0.0006	0.0117	0.0034	0.0021
	5:1	0.0009	0.0003	0.0002	0.0018	0.0007	0.0004	0.0173	0.0031	0.0015

(b) $\hat{s}$ of ζ_L

ϵ		.00625			.25			1		
N		75	150	300	75	150	300	75	150	300
TSR	2:1	0.0342	0.0137	0.0047	0.0730	0.0314	0.0144	0.0947	0.0336	0.0137
	3:1	0.0271	0.0032	0.0015	0.0233	0.0058	0.0027	0.2866	0.1738	0.0078
	4:1	0.0118	0.0026	0.0012	0.0121	0.0053	0.0024	0.0552	0.0111	0.0050
	5:1	0.0059	0.0022	0.0011	0.0108	0.0047	0.0023	0.0343	0.0103	0.0049

(c) $\hat{s}$ of η_S

ϵ		.00625			.25			1		
N		75	150	300	75	150	300	75	150	300
TSR	2:1	0.0885	0.0621	0.0461	0.1407	0.0901	0.0450	0.2615	0.1277	0.0672
	3:1	0.0247	0.0168	0.0137	0.0440	0.0315	0.0199	0.1603	0.0621	0.0371
	4:1	0.0229	0.0167	0.0152	0.0414	0.0308	0.0219	0.1753	0.0802	0.0482
	5:1	0.0184	0.0145	0.0142	0.0390	0.0251	0.0234	0.6476	0.0762	0.0416

(d) $\hat{s}$ of ζ_S

ϵ		.00625			.25			1		
N		75	150	300	75	150	300	75	150	300
TSR	2:1	3.4059	4.0684	1.8926	4.6965	5.1164	3.9750	5.8324	5.2429	3.6741
	3:1	0.0060	0.0028	0.0014	0.0141	0.0058	0.0029	0.6863	0.0194	0.0088
	4:1	0.0062	0.0029	0.0013	0.0143	0.0061	0.0025	0.3213	0.0223	0.0081
	5:1	0.0062	0.0028	0.0011	0.0125	0.0055	0.0026	1.3766	0.0211	0.0071

Table 9: Estimated parametric standard errors by timescale ratio (TSR), total occasions (N), and measurement error (ϵ)

(a) η_L

ϵ		.00625			.25			1		
N		75	150	300	75	150	300	75	150	300
TSR	2:1	0.0109	0.0058	0.0039	0.0183	0.0104	0.0068	0.0336	0.0200	0.0137
	3:1	0.0063	0.0040	0.0027	0.0121	0.0076	0.0051	0.0276	0.0173	0.0107
	4:1	0.0028	0.0017	0.0012	0.0047	0.0029	0.0020	0.0076	0.0048	0.0032
	5:1	0.0017	0.0010	0.0007	0.0028	0.0017	0.0011	0.0046	0.0029	0.0019

(b) ζ_L

ϵ		.00625			.25			1		
N		75	150	300	75	150	300	75	150	300
TSR	2:1	0.0959	0.0538	0.0345	0.1384	0.0809	0.0541	0.1653	0.1220	0.0845
	3:1	0.0288	0.0193	0.0136	0.0505	0.0351	0.0239	0.0967	0.0719	0.0489
	4:1	0.0170	0.0110	0.0076	0.0270	0.0177	0.0123	0.0402	0.0273	0.0190
	5:1	0.0123	0.0077	0.0053	0.0195	0.0131	0.0088	0.0302	0.0211	0.0147

(c) η_S

ϵ		.00625			.25			1		
N		75	150	300	75	150	300	75	150	300
TSR	2:1	0.2531	0.0369	0.0213	0.2266	0.1014	0.0499	0.2503	0.0982	0.0626
	3:1	0.0225	0.0147	0.0100	0.0476	0.0314	0.0210	0.1126	0.0712	0.0488
	4:1	0.0209	0.0134	0.0089	0.0432	0.0275	0.0185	0.1062	0.0658	0.0443
	5:1	0.0187	0.0115	0.0077	0.0379	0.0238	0.0155	0.0911	0.0587	0.0376

(d) ζ_S

ϵ		.00625			.25			1		
N		75	150	300	75	150	300	75	150	300
TSR	2:1	9.6780	2.8344	3.9357	6.6568	7.3476	6.2110	3.4799	1.6611	1.6127
	3:1	0.0336	0.0218	0.0149	0.0739	0.0491	0.0330	0.1987	0.1288	0.0876
	4:1	0.0319	0.0206	0.0138	0.0674	0.0434	0.0294	0.1699	0.1096	0.0744
	5:1	0.0285	0.0177	0.0119	0.0607	0.0386	0.0254	0.1538	0.1015	0.0654